

# Novel First-Principles Insights into Graphene Fluorination

Tahereh Malakoutikhah,\* S. Javad Hashemifar,<sup>†</sup> and Mojtaba Alaei  
*Department of Physics, Isfahan University of Technology, Isfahan 84156-83111, Iran*

Comprehensive first-principles calculations are performed on diverse arrangements of relevant chemical defects in fluorographene to provide accurate microscopic insights into the process of graphene fluorination. The minimum energy paths for the half- and full-fluorination processes are calculated for a better understanding of these phenomena. While experimental observations indicate a much slower rate of the full-fluorination process, compared with the half-fluorination one, the obtained energy profiles demonstrate much enhanced fluorine adsorption after the half-fluorination stage. This ambiguity is explained in terms of significant chemical activation of the graphene sheet after half-fluorination, which remarkably facilitates the formation of chemical contaminants in the system and thus substantially slows down the full-fluorination procedure. After considering the binding energy and durability of the relevant chemical species, including hydrogen, oxygen, and nitrogen molecules and xenon atom, it is argued that oxygen-fluorine ligands are the most likely chemical contaminants opposing the full-fluorination of a graphene sheet. We propose an oxygen desorption mechanism for the atomic description of the full-fluorination procedure in realistic situations. It is argued that the proposed mechanism explains well much enhanced rate of the full-fluorination procedure at elevated temperatures.

PACS numbers:

## I. INTRODUCTION

Fluorographene (FG) is a distinguished member of graphene (Gr) derivatives, which is formed by covering both sides of a Gr sheet with a fluorine monolayer, leading to the  $\text{FC}_2\text{F}$  chemical formula. The applicable properties of FG added to its extraordinary features inherited from pristine graphene, have attracted great interest over the last decade. The stoichiometric FG has an ordered structure that is thermally stable up to  $400^\circ\text{C}$ .<sup>1</sup> The experimental Young modulus of this 2D material is  $100\text{ N/m}$  which shows its high mechanical stability. Finally, what makes FG prominent among others is having the widest measured band gap of about  $3\text{ eV}$  among all of the Gr derivatives.<sup>1</sup> Recent studies confirm its potential applications in batteries and supercapacitors, electrochemical sensors, solar cells, organic field-effect transistors, electrocatalytic oxygen and hydrogen reactions, spintronic devices, anti-corrosion and self-cleaning coatings, oil-water separation, biomedicine, optoelectronic, and photonic.<sup>2</sup>

Fluorination of graphene sheets with a proper chemical agent is a systematic method for the synthesis of stoichiometric FG samples. Xenon difluoride ( $\text{XeF}_2$ ) is a popular fluorinating agent that is utilized for the fluorination of graphene at various temperatures. Nair and colleagues observed that complete fluorination may take more than two weeks at  $70^\circ\text{C}$ , while at  $200^\circ\text{C}$  about 10 hours is enough to obtain full-fluorinated samples.<sup>1</sup> Creutzburg et al. performed the same procedure at  $120^\circ\text{C}$  and found that after about 48 hours the Gr samples are fully fluorinated.<sup>3</sup> Kashtiban and others employed accurate electron microscopies to distinguish two stages in the fluorination procedure. They argue that in the first stage, one side of the Gr sheet is rapidly fluorinated (half-fluorination stage) and then the fluorination of the oppo-

site side will be started (full-fluorination stage).<sup>4</sup> These experimental results suggest the presence of some nontrivial and temperature-dependent mechanism against the adsorption of fluorine atoms on the graphene sheet, in the second fluorination stage. A theoretical molecular dynamics (MD) simulation further complicates the situation, as it shows that adsorption of a fluorine atom on a Gr sheet encourages adsorption of a second fluorine atom at the opposite side of the sheet.<sup>5</sup> Another discrepancy is the theoretical band gap of FG which is much higher than the measured one. While the experimental band gap of FG is expected to be in the range of  $3\text{--}3.8\text{ eV}$ ,<sup>1,6</sup> the most accurate first-principles techniques predict a band gap of  $5.1\text{--}7.49\text{ eV}$  for this 2D system.<sup>7–10</sup> Considering some kinds of defects may somewhat reduce the theoretical band gap of FG toward the experimental value.<sup>10,11</sup>

The nontrivial ambiguities observed in fluorographene suggest possible misunderstanding in the graphene fluorination process. Hence, in this work, we employ accurate first-principles calculations to provide new microscopic insights for a more precise understanding of the graphene fluorination procedure.

## II. METHOD

Our electronic structure calculations and structural relaxations were performed in the framework of density functional theory by using the full potential numeric atom-center orbital (NAO) technique implemented in the FHI-aims package.<sup>12</sup> The NAO basis functions:

$$\varphi_i(r) = \frac{u_i(r)}{r} Y_{lm}(\omega) \quad (1)$$

are composed of radial solutions  $u_i(r)$  of a Schrödinger-like equation and spherical harmonics  $Y_{lm}$ . The numer-

ically tabulated functions,  $u_i(r)$ , are proven to be very efficient for accurate simulation of non-periodic and periodic systems.

For simulating the 2D sheets, we use a slab supercell containing a vacuum thickness of about 15 Å, to prevent artificial interactions between adjacent layers. Among possible atomic configurations for FG, we adopt the chair structure, sketched in Fig. 2, which is argued to be the lowest energy configuration of this 2D material. A mesh of  $8 \times 8 \times 1$  k-points was used for our Brillouin zone integrations and the PBEsol exchange-correlation functional was employed for our structural optimizations.<sup>13</sup> The scalar relativistic atomic-ZORA approximation (zero-order regular approximation) was implemented to involve the relativistic effects,<sup>14</sup> while the full relativistic spin-orbit effect was only considered for the adsorption of the heavy Xe element. Moreover, the van der Waals correction based on the Hirshfeld partitioning of the electron density and spin polarization was considered in the calculations.<sup>15</sup>

### III. RESULTS AND DISCUSSIONS

As it was mentioned in the Introduction, a major experimental observation in the FG synthesis is that fluorination of the second side of the system takes weeks to be completed<sup>4</sup> and it is significantly accelerated by increasing temperature from 70 to 200°C.<sup>1</sup> This observation may be attributed to the appearance of an energy barrier for the adsorption of fluorine atoms on the opposite side of a half-fluorinated graphene (hFG) sheet. Hence, in the first step, we calculated and compared the adsorption energy path of a fluorine atom on a pristine and a half-fluorinated Gr sheet. In this regard, the energy of the system was minimized at several F atom-sheet distances by constrained relaxation of the atomic positions and unit cell parameters, in a  $2 \times 2$  slab supercell. The obtained energy path diagrams, presented in Fig. 1, indicate no energy barrier for the adsorption of the fluorine atom on either the pristine or the half-fluorinated Gr sheet. Moreover, the adsorption energy of the fluorine atom on hFG is remarkably enhanced with respect to the pristine sheet, in agreement with a recent MD simulation.<sup>5</sup> These observations sound inconsistent with the very low experimentally observed rate of the full-fluorination process of graphene.<sup>1</sup> Therefore, we propose a different scenario to explain this discrepancy.

The much higher binding energy of a fluorine atom on hFG, compared with the pristine Gr, indicates that the adsorption of a fluorine layer on a graphene sheet significantly activates the opposite facet of the sheet for adsorbing chemical species. Therefore, the opposite facet of the hFG sheet is expected to be suddenly contaminated with available chemical species in the environment. In other words, on the opposite side of hFG, close competition is expected between the fluorine atoms and other available chemical species to occupy the free adsorption sites of

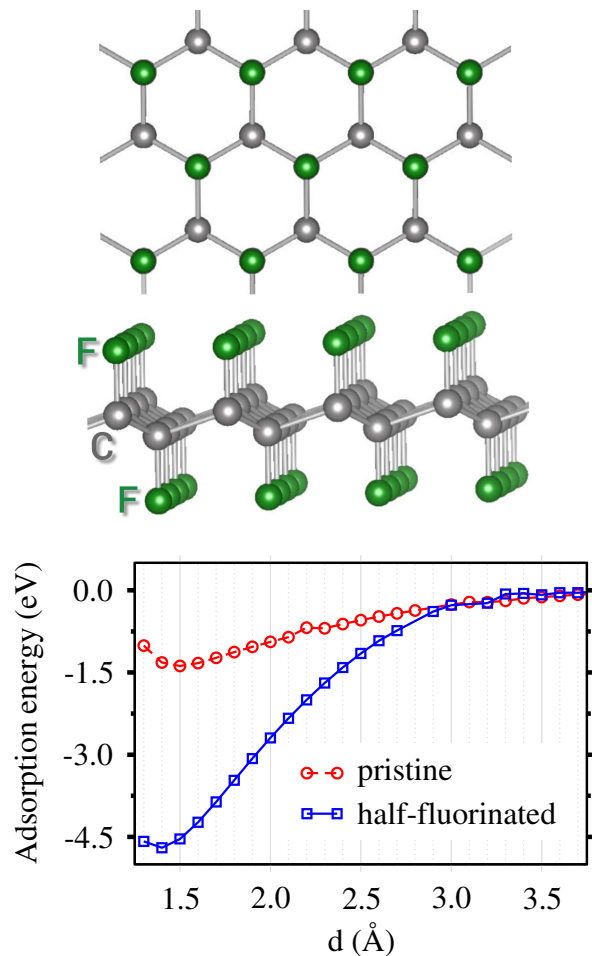


FIG. 1: Top and side views of the chair structure of a fluorographene monolayer ( $\text{FC}_2\text{F}$ ) and the calculated adsorption energy path of a fluorine atom on a pristine graphene sheet and a half-fluorinated one.

the sheet. This competition is anticipated to be the main mechanism for slowing the rate of the full-fluorination of a Gr sheet. Moreover, the presence and persistence of unwanted chemical species in the adsorption sites of FG may explain the large difference between the theoretical and experimental band gap of the system.

To verify this scenario, we considered the adsorption of four inert chemical species (Xe atom and  $\text{H}_2$ ,  $\text{N}_2$ , and  $\text{O}_2$  molecules) on the pristine and the half-fluorinated graphene sheet. These natural molecules are available in the dry atmosphere of a glove box used for the traditional fluorination of Gr samples. The adsorption of these species was studied in a  $2 \times 2$  lateral supercell (Fig. 2) to reduce the effects of the adjacent replicas. The obtained relaxed geometries are sketched in Fig. 2 and the computed physical parameters are presented in table I. We observe the physical adsorption of these inert species on the pristine sheet ( $\text{C}_8$ ), the corresponding absolute adsorption energies are below 0.2 eV, whereas the bond lengths are above 2.6 Å. In the case of the heavy Xe atom, we considered the spin-orbit correction and found

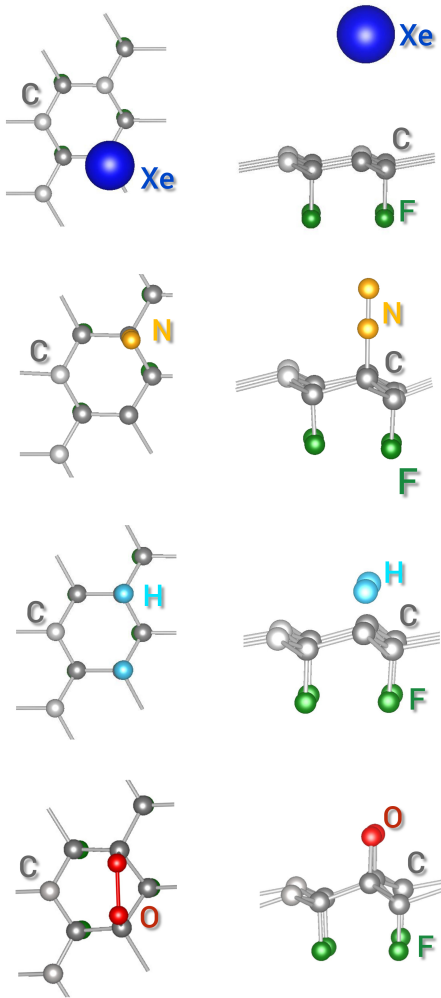


FIG. 2: Top and side views of the relaxed structures of the hFG sheet, after adsorption of different chemical species.

a negligible relativistic effect in the corresponding binding energy. These observed low binding energies may be well compensated by the room temperature vibrational energy of the adsorbate atoms as well as by the kinetic energy of the incident F atoms during the fluorination process. To speculate the vibrational energy of the adsorbates, we calculated the gamma point vibrational modes of the xenon atom, adsorbed on the pristine ( $C_8$ ) sheet. The results indicate three soft modes at about 6, 10, and 31  $\text{cm}^{-1}$ , all below 4 meV. These soft modes are well saturated at room temperature and hence the corresponding vibrational energy would be  $3k_B T$ , which equals about 0.08 eV at room temperature. Similarly, a diatomic molecule physically adsorbed on graphene, is expected to have five soft vibrational modes and hence the corresponding room temperature vibrational energy should be roughly about 0.13 eV. Adapting a Maxwell-Boltzmann distribution for the incident F atoms (Fig. 3), we observe that at the temperature of 70°C about 8% of the F atoms have a kinetic energy higher than 0.1 eV.

TABLE I: Obtained equilibrium parameters of the pristine ( $C_8$ ) and the half-fluorinated ( $F_4/C_8$ ) graphene sheet after adsorption of various chemical species, including F and Xe atoms and  $N_2$ ,  $O_2$ , and  $H_2$  molecules;  $E_b$  (eV): binding energy,  $2a$  (Å): equilibrium lattice parameter of the supercell,  $d$  (Å): equilibrium molecule-sheet vertical distance. In two more important cases, a larger  $4 \times 4$  supercell ( $F_{16}/C_{32}/F_{14}O_2$ ) is also considered. In these cases, the equilibrium lattice parameter is divided by two, to be comparable with the other results. It should be clarified that the binding energy and vertical distance have been calculated for the last chemical species written in the first column.

system	$E_b$	$2a$	$d$
$C_8$	—	4.915	—
$C_8/F$	-2.06	4.927	1.492
$C_8/Xe$	-0.16	4.914	3.920
$C_8/N_2$	-0.12	4.923	2.953
$C_8/O_2$	-0.09	4.914	2.650
$C_8/H_2$	-0.05	4.917	2.808
$F_4/C_8/F$	-5.46	5.079	1.420
$F_4/C_8/Xe$	-0.18	5.070	3.764
$F_4/C_8/N_2$	-0.34	5.085	1.395
$F_4/C_8/H_2$	-4.67	5.095	1.106
$F_4/C_8/O_2$	-3.97	5.071	1.334
$F_4/C_8/F_1N_2$	-0.29	5.097	1.402
$F_4/C_8/F_2N_2$	+0.00	5.118	1.409
$F_4/C_8/F_3N_2$	-0.12	5.167	3.568
$F_4/C_8/F_1O_2$	-3.49	5.124	1.324
$F_4/C_8/F_2O_2$	-3.27	5.174	1.332
$F_{16}/C_{32}/F_{14}O_2$	-2.38	5.158	1.307
$F_4/C_8/F_2(OH)_2$	-4.44	5.180	1.399
$F_4/C_8/F_2(OF)_2$	-2.29	5.212	1.333
$F_{16}/C_{32}/F_{14}(OF)_2$	-3.08	5.179	0.961

Therefore, we conclude that the thermal vibrational energies and the kinetic energy of the incident F atoms at 70°C are sufficient to clean up the surface of the pristine graphene from the weakly bounded chemical contaminants (table I) and consequently give rise to a fast half-fluorination process for the pristine graphene at 70°C.

The obtained binding energies on hFG ( $F_4/C_8$ ) exhibit a clear enhancement with respect to the corresponding values on the pristine graphene. This observation confirms the proposed scenario about the chemical activation of the second facet of graphene after half-fluorination. The largest activation is seen for the  $O_2$  and  $H_2$  molecules where experience a tight chemical bonding to the half-fluorinated graphene. As it is seen in Fig. 2, both molecules prefer a parallel configuration to the sheet. In the case of  $H_2$  molecule, the hydrogen atoms are almost decoupled on the sheet, and each one binds to its underlying carbon atom. On the other hand, oxygen

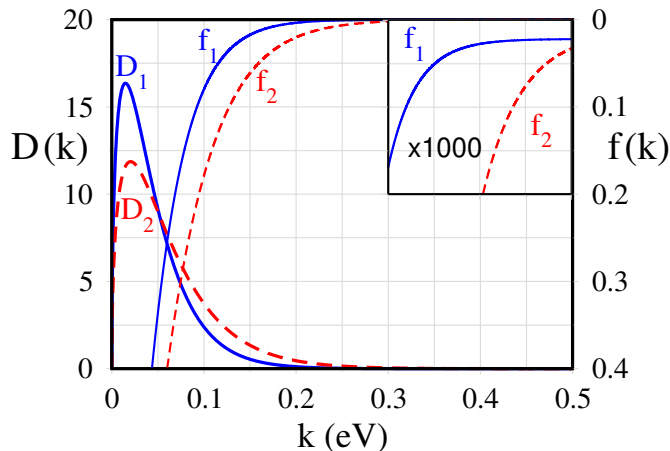


FIG. 3: Maxwell-Boltzmann distribution  $D(k)$  as a function of the particle kinetic energy  $k$  at 70°C ( $D_1$ ) and 200°C ( $D_2$ ), and the resulting fraction of particles  $f(k)$  with a kinetic energy above  $k$  ( $f(k) = \int_k^\infty D(k')dk'$ ). The inset shows the enlarged tail of the  $f(k)$  functions.

atoms keep their bonding on the graphene sheet and thus slightly deviate from the carbon top sites. Although  $N_2$  exhibits much weaker binding to  $F_4/C_8$ , compared with  $O_2$  and  $H_2$ , it is still significantly enhanced with respect to the  $N_2$  binding on the pristine graphene ( $C_8$ ). Moreover, this molecule prefers a vertical alignment on the sheet (Fig. 2). The Xe atom shows the lowest binding enhancement, after half-fluorination of graphene. The stable position of this noble element on  $F_4/C_8$  is the carbon top site, while on  $C_8$  it prefers the hollow sites of the sheet. Comparing the binding energy of F and other investigated species on  $F_4/C_8$  (table I) clarifies the anticipated competition between these species to occupy the adsorption sites of the second facet of the hFG. In our proposed scenario, this competition is the main reason behind the very slow rate of the full-fluorination process of graphene. It should be stressed that the main competition likely happens between oxygen molecules and F atoms, because of the close binding energy of these entities. Although  $H_2$  has closer binding energy to the fluorine atom, the very low amount of hydrogen in the environment rules out its significant impact on the fluorination process. However, our data suggest the presence of rare hydrogen defects in the fluorographene samples which may have nontrivial influences on the electronic structure of the system. It may also be noted that  $N_2$  and  $H_2$  exhibit a second stationary position on  $F_4/C_8$  which involves much weaker bonding relative to the first one discussed above. In the case of  $N_2$ , this weaker bonding happens about  $3.5\text{\AA}$  above the sheet with a binding energy of  $-0.11\text{ eV}$ , while,  $H_2$  displays a second stationary position around  $2.73\text{\AA}$  above the sheet with a similar binding energy of  $-0.11\text{ eV}$ .

Now, we can explain some important observations about graphene fluorination in the dry atmosphere of a glove box.<sup>1</sup> It should be noted that the graphene sheets

were assembled on a gold grid to make both sides of the sheet exposable to F atoms. However, one side of the sheet is practically more accessible to the available adsorbates. Hence, in the first stage, one side of graphene is rapidly fluorinated, because available chemical species are not able to compete with the fluorine atoms for occupying the adsorption site of the sheet. The half-fluorination process significantly increases the chemical activity of the opposite facet of the sheet and hence in addition to the fluorine atoms, mainly the oxygen molecules and to a lower extent, the nitrogen molecules also occupy the adsorption sites of the hFG sheet and thus remarkably slow down the full-fluorination process. Our scenario predicts very fast full-fluorination of graphene in an oxygen-free ambient, confirmed by a very recent experiment. Li and others observed very a high rate of fluorographene synthesis at a vacuum condition of  $10^{-6}$  mbar.<sup>16</sup> Moreover, the observation of the high chemical activity hFG rules out the stability and feasibility of the individual half-fluorinated graphene samples.

In the next step, we investigate the durability of  $N_2$  and then  $O_2$  impurities in the fluorographene samples. The gamma point vibrational frequencies of an  $N_2$  molecule adsorbed on  $C_8$  and  $F_4/C_8$  were estimated to be (12,18,57,94,96) and (10,20,36,49,50)  $\text{cm}^{-1}$ , respectively, which in both cases give rise to a thermal energy of about 0.15 and 0.20 eV at 70 and 200°C, respectively. These thermal energies are not sufficient to compensate for the binding energy of an individual  $N_2$  molecule ( $-0.34\text{ eV}$ ) on hFG (table I). In order to provide more information, we investigated the accumulation of F atoms and other chemical species in the neighborhood of an adsorbed  $N_2$  molecule on the hFG. In the first step, we found that  $N_2$  molecule does not permit adsorption of a further  $N_2$  in the adjacent sites. Then, we studied the adsorption of F atoms in the neighborhood of an  $N_2$  molecule (table I). This procedure was seen to weaken the binding of  $N_2$  molecule to the hFG. Adsorption of one F atom ( $F_4/C_8/F_1N_2$ ) increases the binding energy of  $N_2$  molecule to  $-0.29\text{ eV}$  while adsorption of two F atoms ( $F_4/C_8/F_2N_2$ ) almost decouple the  $N_2$  molecule from the sheet. Adsorption of the third F atom shifts the molecule to its second stationary position which is about  $3.56\text{\AA}$  far above the sheet and thus may be easily removed by thermal effects. It should also be noted that an  $N_2$  adsorbate on  $F_4/C_8$  has a slight influence on the binding of F atoms in the adjacent sites. The binding energy of the first, the second, and the third F atom in the vicinity of  $N_2$  is  $-5.41$ ,  $-5.20$ , and  $-5.45\text{ eV}$  which are pretty close to the binding energy ( $-5.46\text{ eV}$ ) of an individual F atom on the clean facet of the hFG (table I). These results show that while individual  $N_2$  adsorbates on hFG are rather stable, the prior accumulation of F atoms in their vicinity detaches these molecules from the surface, even at low temperatures of about 70°C.

The same scheme was applied around an  $O_2$  adsorbate on the hFG. First, we found that this adsorbate significantly increases the binding energy of a further oxy-

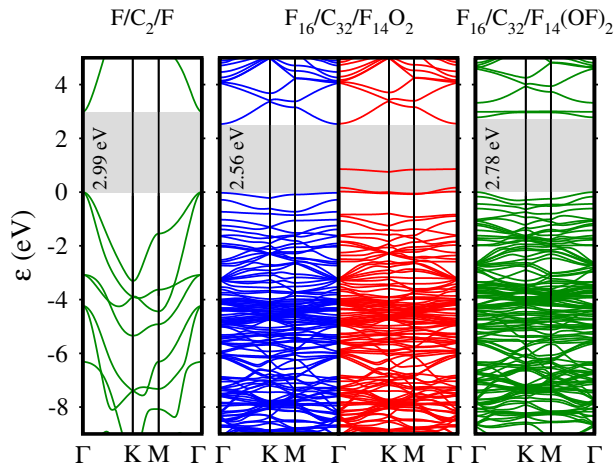


FIG. 4: Obtained band structures for  $F/C_2/F$  (fluorographene),  $F_{16}/C_{32}/F_{14}O_2$ , and  $F_{16}/C_{32}/F_{14}(OF)_2$ .  $F_{16}/C_{32}/F_{14}O_2$  exhibits a spin polarized band structure, blue and red colors show spin majority and spin minority states, respectively. The shaded areas show the band gap region and the band gap values are written in the figures.

gen molecule in the adjacent sites to a value of about  $-1.05$  eV. Then, adsorption of F atoms was considered around the  $O_2$  molecule. Because of the parallel configuration of  $O_2$  on the hFG, only two F atoms may be adsorbed in the vicinity of  $O_2$  in a  $2 \times 2$  supercell. The first and the second F atoms increase the binding energy of oxygen to  $-3.49$  and  $-3.27$  eV, respectively (table I). Despite these weakening effects, the  $O_2$  molecule is still tightly attached to the sheet and thermal effects are far lower to compensate for the remained binding energy. In order to reduce the effects of adjacent  $O_2$  molecules, we repeated the last calculation in a larger  $4 \times 4$  supercell and found a high binding energy of about  $-2.38$  eV for the  $O_2$  molecule fully surrounded by F atoms ( $F_{16}/C_{32}/F_{14}O_2$ ). These findings argue that the complete elimination of the oxygen defects from the fluorographene samples is an elaborating task. This observation may explain the observed rare difference between the experimental ( $3.1$ - $3.8$  eV)<sup>6</sup> and the theoretical excitonic band gap of this system ( $5.1$  eV).<sup>10</sup> The obtained spin polarized band structure of  $F_{16}/C_{32}/F_{14}O_2$  is compared with that of an ideal FG sample in Fig. 4. It is seen that  $O_2$  impurities may significantly decrease the theoretical band gap of FG, obtained within the single-particle Kohn-Sham framework.<sup>17</sup> Moreover, some minority spin states occupy the band gap and cross the Fermi level of the oxygen defected FG, indicating the chemical activity of the oxygen defect in this system.

After confirming the very probable presence of  $O_2$  defects in the FG samples, we considered their chemical activity by adsorbing a further  $H_2$  and  $F_2$  molecule on top of these defects. The obtained results, presented in table I, exhibit the rather high chemical activity of this point defect. The binding energy of  $H_2$  on  $O_2$  is about

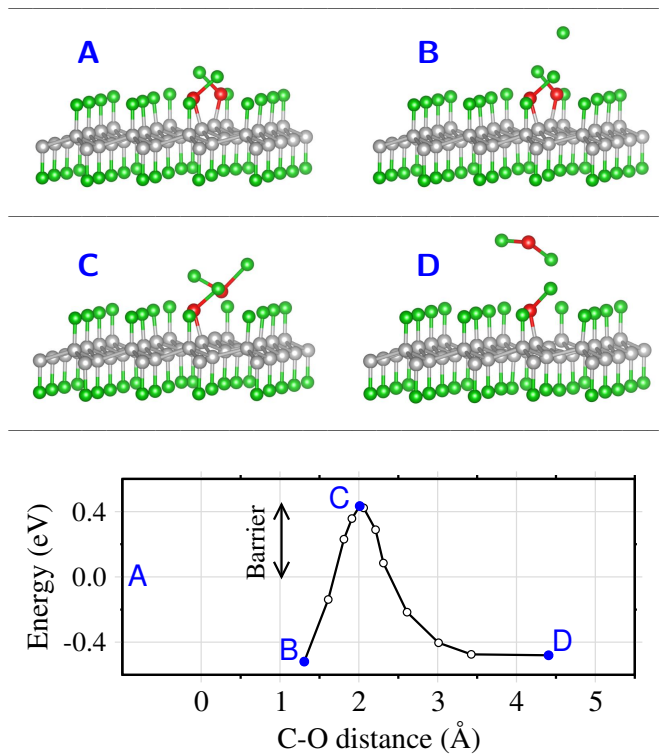


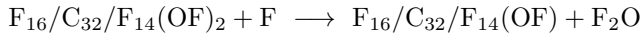
FIG. 5: A: predicted atomic configuration of an oxygen defected FG in a  $4 \times 4$  supercell ( $F_{16}/C_{32}/F_{14}(OF)_2$ ). The red, green, and gray balls stand for the oxygen, fluorine, and carbon atoms, respectively. B, C, D: initial, transition state, and final configurations of the  $F_{16}/C_{32}/F_{14}(OF)_2 + F$  complex in the proposed oxygen desorption reaction. bottom: optimized energy path of the oxygen desorption reaction as a function of the reaction coordinate.

$-4.44$  eV and we observed that this strong binding almost decouples the two H atoms from each other. The binding of  $F_2$  on  $O_2$  is also predicted to be rather strong, each F atom attaches to one of the O atoms with a binding energy of about  $-1.13$  eV/atom. Because of the much higher abundance of F atoms in the FG synthesis environment, compared with the  $H_2$  molecules, the anticipated  $O_2$  defects in FG are likely covered by further F atoms, leading to the pairs of OF ligands. In order to approach the more realistic situations, we optimized the atomic configuration of these ligands in a larger  $4 \times 4$  supercell (Fig. 5) and observed a cross geometry in the neighboring OF ligands. The electronic band structure of this system is also calculated and presented in Fig. 4. Compared with the system with a bare oxygen defect ( $F_{16}/C_{32}/F_{14}O_2$ ), we observe that the semiconducting feature of FG is well recovered with a band gap of about  $2.78$  eV, that it is still about 7% lower than the ideal FG.

In the last part of the paper, we provide some first-principles arguments about the significant enhancement of the full-fluorination procedure of graphene in the glove box, after increasing the temperature from  $70^\circ\text{C}$  to  $120^\circ\text{C}$  and  $200^\circ\text{C}$ .<sup>1,3</sup> According to the above discus-



sions, neighboring OF ligands are the most likely defects in the FG samples, hence the full-fluorination process requires an effective mechanism for removing the adsorbed oxygen atoms. We focus on the optimized model of an oxygen defected FG sample in a  $4 \times 4$  supercell (Fig. 5) and propose the following oxygen desorption reaction:



An incident F atom picks up one of the OF ligands from the sample and forms a free  $\text{F}_2\text{O}$  molecule. In order to calculate the energy barrier of this reaction, we selected the vertical distance between the oxygen atom of the target ligand and its underlying carbon atom (C-O distance) as the reaction coordinate and then optimized the energy of the system at different values of this coordinate. The obtained reaction energy path is presented in Fig. 5. Four configurations are labeled in the energy path and sketched in the figure for a better understanding of the oxygen desorption reaction. As it was mentioned, the configuration A represents the predicted structure of the oxygen defected FG in a  $4 \times 4$  supercell. The minimized energy of this system plus the energy of a free F atom has been selected as the reference of energy in the reaction energy path. The configuration B shows an equilibrium position of the incident F atom above the ligand, however, the kinetic energy of the atom prevents it from stopping at this position. Hence, the incident F atom may approach and then attach to the target OF ligand to form an  $\text{F}_2\text{O}$  molecule on the surface. If the incident F atom has enough kinetic energy, the formed molecule at the surface may climb the energy barrier to reach the transition configuration C, where the oxygen atom of the V-shape  $\text{F}_2\text{O}$  molecule is about  $2 \text{ \AA}$  above the central graphene layer (Fig. 5). On the other hand, in the final configuration D, the desorbed  $\text{F}_2\text{O}$  molecule exhibits an inverted V-shape geometry. Our results indicate an energy barrier of about  $0.43 \text{ eV}$  for the proposed oxygen desorption reaction. It should be noted that the activation barrier should be calculated from A, not B that is an intermediate configuration of the reaction.

In our proposed oxygen desorption reaction, the incident F atom should have a kinetic energy of at least  $0.43 \text{ eV}$ , to overcome the activation barrier of the reaction. According to the Maxwell-Boltzmann distribution (Fig. 3), at  $70^\circ\text{C}$  only about  $2.5 \times 10^{-3} \%$  of the particles have a kinetic energy above  $0.43 \text{ eV}$ , which may explain the very low rate of the full-fluorination of graphene at this temperature. Nair and others found that complete fluorination of a graphene sheet at  $70^\circ\text{C}$  takes more than two weeks, while at  $200^\circ\text{C}$  about 10 hours is enough for the full-fluorination procedure.<sup>1</sup> At  $200^\circ\text{C}$ , the number of particles with enough kinetic energy increases by a factor of about 4 (Fig. 3), which qualitatively confirms the mentioned rate enhancement. However, a more accurate comparison of the reaction rate ( $k(T)$ ) at different temperatures requires the Arrhenius scheme:

$$k(T) = Ae^{-E_a/k_B T}$$

$A$ ,  $E_a$ ,  $k_B$ , and  $T$  are frequency factor, activation energy, the Boltzmann constant, and the Kelvin temperature, respectively. Inserting the obtained activation energy ( $0.43 \text{ eV}$ ) and neglecting the temperature dependence of the frequency factor, the above equation predicts that the reaction rate at  $200^\circ\text{C}$  is about 55 times higher, compared with  $70^\circ\text{C}$ . Hence the more than two weeks (336 hours) full-fluorination procedure of graphene at  $70^\circ\text{C}$ , is expected to reduce to more than 6 hours at  $200^\circ\text{C}$ , in close agreement with the observation of Nair and colleagues ( $\sim 10$  hours).<sup>1</sup> In the same way, the full-fluorination time at  $120^\circ\text{C}$  is predicted to be more than 39 hours, well consistent with the very recent record of Creutzburg et al. (48 hours).<sup>3</sup> Therefore, our proposed oxygen defected FG and oxygen desorption mechanism explain well the observed features in the graphene fluorination procedure.

#### IV. CONCLUSIONS

In this work, we performed extensive full-potential DFT calculations on various arrangements of the relevant atomic and molecular defects in fluorographene (FG) to understand the experimentally observed two stages fluorination procedure of Gr. In a glove box, at  $70^\circ\text{C}$  the half-fluorination of a pristine graphene sheet was found to happen quickly while the full-fluorination procedure takes more than two weeks. In the first step, the adsorption energy profile of a fluorine atom on the pristine and half-fluorinated graphene (hFG) sheet was calculated and compared to identify a significant enhancement in the chemical activity of graphene after the half-fluorination stage. This observation rules out the feasibility of individual half-fluorinated graphene samples. Afterward, adsorption of the relevant chemical species, including Xe atom and  $\text{N}_2$ ,  $\text{O}_2$ , and  $\text{H}_2$  molecules were considered on the pristine and half-fluorinated graphene to confirm the predicted chemical activation. After considering various arrangements of the adsorbed  $\text{N}_2$  molecule on FG, it was argued that this point defect is not durable and typical thermal energies at  $70^\circ\text{C}$  are enough to clean up the FG samples from this defect. On the other hand, the  $\text{O}_2$  molecule exhibits a different behavior and may form thermally stable defects in FG. We calculated diverse configurations of this molecule and concluded that pairs of OF ligands with a cross geometry are likely the most abundant impurities in the realistic FG samples, opposing the full-fluorination procedure. We proposed an oxygen desorption reaction for removing the OF ligands from the sample and thus enhancing the complete fluorination of graphene. In this mechanism, an incident F atom with enough kinetic energy attaches to an OF ligand to form an  $\text{F}_2\text{O}$  molecule on the sheet. This molecule then should overcome an energy barrier of about  $0.43 \text{ eV}$  to leave the sample. These results explain very well the substantially increased rate of the full-fluorination procedure at  $120$  and  $200^\circ\text{C}$ .

## V. ACKNOWLEDGMENTS

The authors appreciate the useful comments of Dr. Mehdi Abdi from Isfahan University of Technology

(IUT). This work was supported by the IUT Vice-Chancellor in Research Affairs.

---

\* Electronic address: t.malakoutikhah@gmail.com

† Electronic address: hashemifar@iut.ac.ir

<sup>1</sup> R. R. Nair, W. Ren, R. Jalil, I. Riaz, V. G. Kravets, L. Britnell, P. Blake, F. Schedin, A. S. Mayorov, S. Yuan, et al., *Small* **6**, 2877 (2010).

<sup>2</sup> D. D. Chronopoulos, A. Bakandritsos, M. Pykal, R. Zbořil, and M. Otyepka, *Applied Materials Today* **9**, 60 (2017).

<sup>3</sup> S. Creutzburg, M. Mergl, R. Hübner, I. Jirka, D. Erb, R. Heller, A. Niggas, P. Grande, F. Aumayr, R. Wilhelm, et al., *Physical Review Materials* **5**, 074007 (2021).

<sup>4</sup> R. J. Kashtiban, M. A. Dyson, R. R. Nair, R. Zan, S. L. Wong, Q. Ramasse, A. K. Geim, U. Bangert, and J. Sloan, *Nature Communications* **5**, 1 (2014).

<sup>5</sup> R. Paupitz, P. Autreto, S. Legoas, S. G. Srinivasan, A. Van Duin, and D. Galvao, *Nanotechnology* **24**, 035706 (2012).

<sup>6</sup> K.-J. Jeon, Z. Lee, E. Pollak, L. Moreschini, A. Bostwick, C.-M. Park, R. Mendelsberg, V. Radmilovic, R. Kostecki, T. J. Richardson, et al., *Acs Nano* **5**, 1042 (2011).

<sup>7</sup> H. Şahin, M. Topsakal, and S. Ciraci, *Physical Review B* **83**, 115432 (2011).

<sup>8</sup> O. Leenaerts, H. Peelaers, A. Hernández-Nieves, B. Partoens, and F. Peeters, *Physical Review B* **82**, 195436 (2010).

<sup>9</sup> W. Wei and T. Jacob, *Physical Review B* **87**, 115431

(2013).

<sup>10</sup> S. Yuan, M. Rösner, A. Schulz, T. O. Wehling, and M. I. Katsnelson, *Physical Review Letters* **114**, 047403 (2015).

<sup>11</sup> L.-y. Huang, X. Zhang, M. Zhang, and G. Lu, *The Journal of Physical Chemistry C* **121**, 12855 (2017).

<sup>12</sup> V. Blum, R. Gehrke, F. Hanke, P. Havu, V. Havu, X. Ren, K. Reuter, and M. Scheffler, *Computer Physics Communications* **180**, 2175 (2009).

<sup>13</sup> J. P. Perdew, A. Ruzsinszky, G. I. Csonka, O. A. Vydrov, G. E. Scuseria, L. A. Constantin, X. Zhou, and K. Burke, *Phys. Rev. Lett.* **100**, 136406 (2008), URL <https://link.aps.org/doi/10.1103/PhysRevLett.100.136406>.

<sup>14</sup> E. van Lenthe, E.-J. Baerends, and J. G. Snijders, *The Journal of Chemical Physics* **101**, 9783 (1994).

<sup>15</sup> A. Tkatchenko, R. A. DiStasio Jr, R. Car, and M. Scheffler, *Physical Review Letters* **108**, 236402 (2012).

<sup>16</sup> H. Li, T. Duan, S. Haldar, B. Sanyal, O. Eriksson, H. Jafri, S. Hajjar-Garreau, L. Simon, and K. Leifer, *Applied Physics Reviews* **7**, 011403 (2020).

<sup>17</sup> Unfortunately, we were not able to verify this trend in the excitonic or quasiparticle band gaps, because our computational resources are not powerful enough to apply first principles GW or excitonic calculations to our rather large supercells.